Chapter 2

Physics Goals and Requirements

2.1 EIC Context and History

The Electron-Ion Collider is a major new research facility to advance the long term vision for Nuclear Physics to discover and understand the emergent phenomena of Quantum Chromo-Dynamics (QCD). The developing of the physics case for the EIC has been a tremendous community effort over the last few decades.

A joint report on the EIC Science case was put together at the Institute for Nuclear Theory (INT) in 2010 [3]. This set the base for the following release in 2014 of a White Paper (WP) [4] outlining the fundamental questions that would have been addressed at the EIC. In the following year, the US 2015 Long Range Plan for Nuclear Science recommended a high-energy high-luminosity polarized EIC as the highest priority for new facility construction.

In 2016, the worldwide fast growing community of scientists interested in the EIC organized itself under the EIC Users Group (EICUG) [www.eicug.org].

In 2017, the National Academy of Sciences, Engeneering, and Medicine (NAS) assessed the science case of the EIC as "compelling, fundamental, and timely". Quoting from the NAS report [5] released in 2018, the EIC can uniquely address three profound questions about nucleons—neutrons and protons—and how they are assembled to form the nuclei of atoms:

- How does the mass of the nucleon arise?
- How does the spin of the nucleon arise?
- What are the emergent properties of dense systems of gluons?

In December 2019, following the extremely positive assessment by the NAS, the US Department of Energy (DoE) established EIC Critical Design 0 (CD0), a "mission need" declaration", formally starting the EIC Project.

At about the same time, in late 2019, the EICUG led an intensive, year-long consideration of the EIC physics measurements and scientific equipment. This initiative yielded the EICUG Yellow Report (YR) [2] defining the detector requirements needed to deliver the science case endorsed by the NAS report and highlighted in the WP and all the subsequent studies and publications. The YR

provided the basis for further development of concepts for experimental equipment best suited for EIC science needs.

The ePIC Collaboration, established in July 2022 at the EICUG Meeting at Stony Brook University. ePIC was born as a merger of two pre-conceptual designs, ECCE [6] and ATHENA [7] and is a general purpose detector to deliver the whole EIC core science program.

The propose of this chapter study key measurements in order to demonstrate that our current detector design, is capable of delivering on its mission.

Processes taken into consideration are chosen for both their relevance to the core science and the specific challenges that they pose to the detector.

All the studies contained in this pre-TDR are based on a full GEANT4 simulation of the ePIC detector and reconstruction tools as available in the October 2024 simulation campaign. As the development of both simulation and tools progresses, we will repeat our studies for the final TDR.

In some instances, our ability to demonstrate the detector performance for a relevant measurement might be hampered by the absence of a needed tool that was yet to be developed/finalized. When this occurs, it must not be taken as that the detector cannot accomplish a certain measurement or that we are overlooking certain physics. Our goal is to be able to show those results by the final version of the TDR (90% design completion).

There are many studies performed by the ePIC's Physics Working Groups that will not enter this selection but that are absolutely relevant for the EIC core science and beyond. Furthermore, many details that went into the physics studies, both on the analysis and the impact on the current knowledge, will be omitted for the purpose of this TDR. The ePIC collaboration plans to separately publish a "science paper" containing all the missing information that cannot be given within the present document.

2.2 The Science Goals of the EIC and the Machine Parameters.

We will add more on science goals and machine parameters here by version 1

2.3 Reconstruction Tools and Special Probes

2.3.1 Kinematic reconstruction

The DIS scattering event can be described by two kinematic variables, typically the momentum transfer squared, Q^2, and scaling variable, x_B. Although it is possible to completely reconstruct neutron-current inclusive event kinematics from only the scattered electron, this does not always result in the best resolution. To optimize resolution, multiple reconstruction methods can be employed, using various combinations of scattered electron and hadronic final state (HFS) information:

- **Electron method**: uses only scattered electron
- $e\Sigma$ **method**: uses both scattered electron and HFS
- **Double-angle method (DA)**: uses both scattered electron and HFS

- **Jacquet-Blondel method (JB)**: uses only HFS

For more details on these three methods see Sec.8.1.1 of the YR [2]. Generally, these methods differ in the calculation of Q^2 and inelasticity y, then the scaling variable is calculated as $x_B = Q^2/sy$. Note that while JB typically does not give the best resolution, it is the only reconstruction method possible for charged-current interactions (where the outgoing DIS lepton is a neutrino).

Figure 2.1 shows the y resolution at ePIC as a function of x_B and Q^2 for 18 GeV on 275 GeV ep collisions. As can be seen, the optimal reconstruction method changes with kinematics. These resolutions result from reconstructing the electron momentum strictly from tracking detectors. The resolution could be further improved by using the electromagnetic calorimeter clusters to reconstruct the electron energy. This is particularly important for electrons scattered into the backwards ECAL.

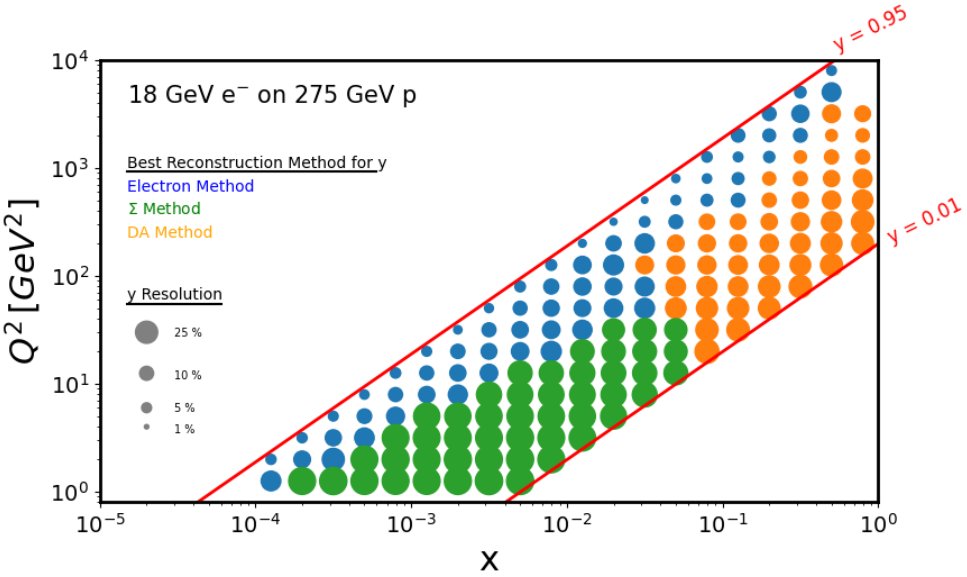

Figure 2.1: Resolution of the inelasticity y, as a function of x and Q^2, when reconstructed using the electron method (blue), Σ method (green), or Double-angle method (orange).

2.3.2 Electron identification and event selection

Regardless of reconstruction method used, it is important to identify the scattered electron in the event final state. It can be challenging to separate the electron signal from the large π^- background present in DIS collisions. A rudimentary electron identification algorithm has been already developed in ePIC and applied to inclusive analyses.

The first step is to separate final state electrons from pions. This is done by applying a cut on E/p, where p is the track momentum and E is the ECAL cluster energy matched to that track. Electrons will typically deposit all of their energy in the ECAL and have $E/p \approx 1$, while pions will pass through the ECAL and peak at $E/p < 1$. The current analysis uses a cut of $0.7 < E/p < 1.3$, which accounts for smearing due to electron energy and momentum resolutions.

The next step is to identify the scattered DIS electron, as other electrons may be present in the final

state. All negative tracks satisfying our E/p requirement are used to calculate $\delta_h = \sum_i (E_i - p_{z,i})$, where the sum i runs over all final-state hadrons. Note that the electron candidate must be excluded in the summation. For the DIS electron, $\delta_h \approx 2E_e$, while for other particles $\delta_h < 2E_e$. The current analysis chooses the electron candidate with the highest δ_h.

This rudimentary algorithm is actively being improved, namely by incorporating signals from PID detectors (hpDIRC, pfRICH, TOF), applying cuts on shower shape parameters of the calorimeter clusters, and using a more rigorous treatment of δ_h instead of simply taking the largest value.

Further, kinematic cuts are applied to ensure DIS kinematics and avoid regions of poor resolution and large backgrounds:

- $Q^2 > 2\,\mathrm{GeV}^2$
- $W^2 > 10\,\mathrm{GeV}^2$
- $0.1 < y < 0.95$

2.3.3 Jets: a versatile probe

As demonstrated in the YR [2], jets are an important observable, bringing both complimentary and unique insight to many of the EIC science goals. In order to comprehensively evaluate the impact that they can have, jet reconstruction has been integrated into the ePIC reconstruction framework, EICrecon. It utilizes the FastJet package to implement various jet definitions. The default settings, which are used for jets saved to the shared output trees and included in the analyses below, include the Anti-k_T algorithm, E-scheme recombination, a resolution of 1.0, and a minimum jet transverse momentum of 1 GeV/c. In addition, constituents were required to have transverse momenta greater than 200 MeV/c to be included in the clustering.

Due to the lack of mature algorithms for integrating information from tracking, calorimetry, and particle identification subsystems, the reconstructed jets used to benchmark the ePIC detector performance and evaluate physics impact are clustered exclusively from charged particle tracks.

The primary metrics for evaluating the quality of jet reconstruction at ePIC are the jet energy scale (JES) and jet energy resolution (JER). These quantities were calculated by comparing the energies of matched particle-level and reconstructed jets. Because the reconstruction currently uses track-only jets and we are primarily interested in quantifying the effects of the detector, only stable charged particles were used when clustering the particle-level jets. For each particle-level jet, the closest reconstructed jet in $\eta - \phi$ space was considered the matching jet as long as $\Delta R = \sqrt{\Delta\eta^2 + \Delta\phi^2}$ was less than 0.1. The quantity: [(reco - particle)/particle] jet energy was found for each set of matching jets and fit with a triple Gaussian function. A triple Gaussian was used to try to take into account the tails of the distribution. The mean of fit is taken as the JES while the sigma is taken as the JER. To get a more differential picture of the jet performance, this procedure was performed as a function of particle-level jet energy for three pseudorapidity ranges as shown in Fig. 2.2.

2.3.4 Exclusive probes: nucleon and nuclei imagining

Among its diverse scientific objectives at the EIC, exclusive reactions and probes play a pivotal role in uncovering the spatial and momentum structure of nucleons and nuclei, as well as in studying their emergent dynamics.

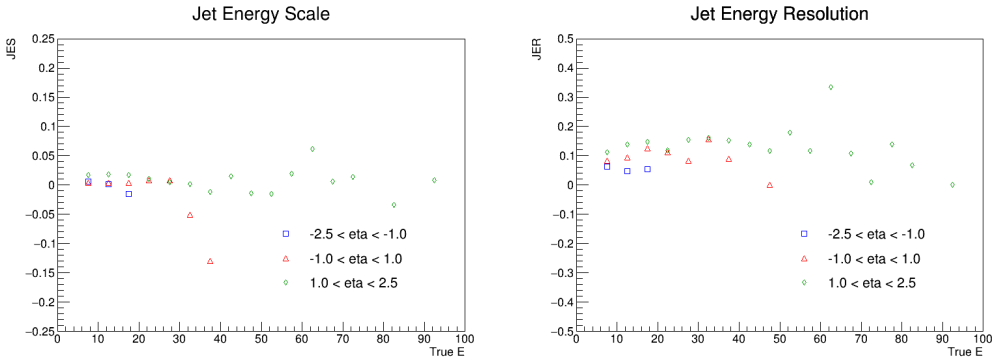

Figure 2.2: PLACEHOLDER (Left) Jet energy scale and (Right) jet energy resolution as a function of particle-level jet energy for backward (blue squares), mid (red triangles), and forward (green diamonds) rapidities.

Exclusive reactions refer to processes where the entire final state of particles is detected, allowing precise reconstruction of the reaction dynamics. These reactions are vital for mapping out Generalized Parton Distributions (GPDs) and exclusive cross-sections, offering a 3D view of the nucleon's internal structure. GPDs encode correlations between parton momentum and spatial position, enabling a tomographic image of the nucleon. The EIC's high luminosity, wide kinematic coverage, and precision detectors make it ideal for studying exclusive channels, such as deeply virtual Compton scattering (DVCS) and exclusive vector meson production.

Deeply Virtual Compton Scattering (DVCS): DVCS is a benchmark process for probing GPDs. In this reaction, an electron scatters off a proton (or nucleus), emitting a high-energy photon while leaving the proton intact. The EIC will provide access to DVCS across a wide range of momentum transfer (t), allowing for detailed studies of the spatial distribution of partons and their evolution with varying energy scales. Precision measurements at the EIC will also test QCD factorization and constrain theoretical models of GPDs, improving our understanding of the spin and angular momentum contributions of quarks and gluons to nucleon spin.

Exclusive Vector Meson Production: This process involves the coherent production of mesons such as ρ, ϕ, J/ψ, and Y in electron-proton or electron-nucleus collisions. At the EIC, measurements of vector meson production will probe gluon distributions at small Bjorken-x, providing insight into gluon saturation effects and the emergence of collective phenomena in QCD. Heavy vector mesons like J/ψ are particularly sensitive to the gluon content of the nucleon, offering a window into the high-density regime of QCD.

In the next subsection, we will highlight three measurements related to nucleon and nucleus imagining: DVCS in ep, exclusive three Upsilon states production in ep, and exclusive Vector Meson production in eA collisions. Based on the YR [2], the requirement for the DVCS in ep is to have a good acceptance of forward proton detection to cover a wide range of t for different x and Q^2 phase spaces above $Q^2 > 1$ GeV^2. For Upsilon productions, the requirement is to have a tracking system

in the main detector to separate the $\Upsilon(1s)$, $\Upsilon(2s)$, and $\Upsilon(3s)$ state. The relative cross section of the different states is the key to this measurement. For the exclusive Vector Meson production, e.g., J/ψ and/or ϕ, the requirement is to have a good momentum resolution to see the dffractive minima and a large acceptance in the far-forward detector to veto the incoherent background contributions.

2.4 The EIC Science (ePIC performance for key observables)

2.4.1 Origin of Nucleon Mass

Nucleons are made of quarks bound together by massless gluons. The Higgs mechanism can only explain the source of the quark masses. Nevertheless, the masses of valence quarks account only for $\sim 1\%$ of a nucleon's mass and thus cannot explain the mass of all the visible matter in the universe. The reminder of the proton mass must originate from the field energy of quarks and gluons in the sea.

The most accessible description of hadrons in terms of their constituent partons is by parton distribution functions (PDFs), representing the fractional (longitudinal) momentum carried by each parton flavor. The inclusive DIS cross section is sensitive to PDFs through the structure functions F_1 and F_2, which are linear combinations of the PDFs.

Tomographic images of quarks and gluons, also achievable at ePIC, will be discussed in Sec.2.4.3.

2.4.1.1 Inclusive neutral current cross sections

To extract neutral-current cross sections, corrections for acceptance and bin migration are defined by comparing reconstructed events to generated events. These corrections are then applied to the reconstructed events. Note that since the same reconstructed events are used for both the corrections and cross section extraction, this by definition yields the cross sections of the underlying event generator.

The projected neutral-current reduced cross sections for three center of mass energies are shown in Figures 2.3-2.5. These use the electron identification and event selection criteria as described in Sec: 2.3.2. However, at this stage the kinematics have been reconstructed using the electron method only. The statistical uncertainties are estimated assuming an integrated luminosity of 10 fb^{-1} for each center of mass energy.

2.4.2 Origin of Nucleon Spin

Thanks to the availability of polarized electron and hadron beams at the EIC, inclusive DIS can be used to probe the contribution of nucleon spin from quark helicity. Double-spin asymmetries between different relative electron/hadron polarization states are sensitive to polarized PDFs through the spin structure function $A_1 \propto g_1 = \sum_q e_q^2(\Delta q - \Delta\bar{q})$. The gluon contribution to nucleon spin is inferred by the Q^2 dependence of the spin structure functions, therefore it is critical for the measurements to cover a wide range of kinematics.

The projected proton double-spin asymmetries A_1^p for three center of mass energies are shown in Figure 2.6. The statistical uncertainties are estimated assuming an integrated luminosity of 10

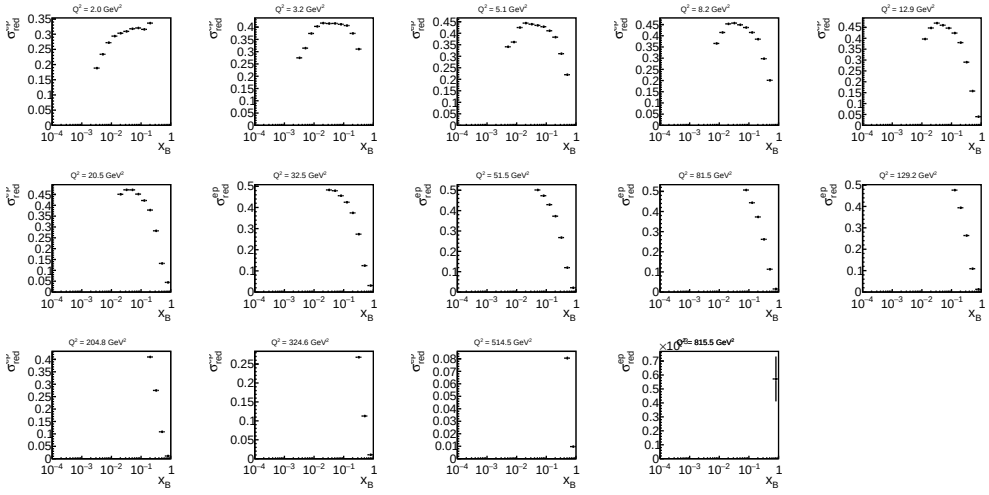

Figure 2.3: Projected *ep* neutral current reduced cross sections at 5x41 GeV. Statistical uncertainties assume an integrated luminosity of 10 fb^{-1}.

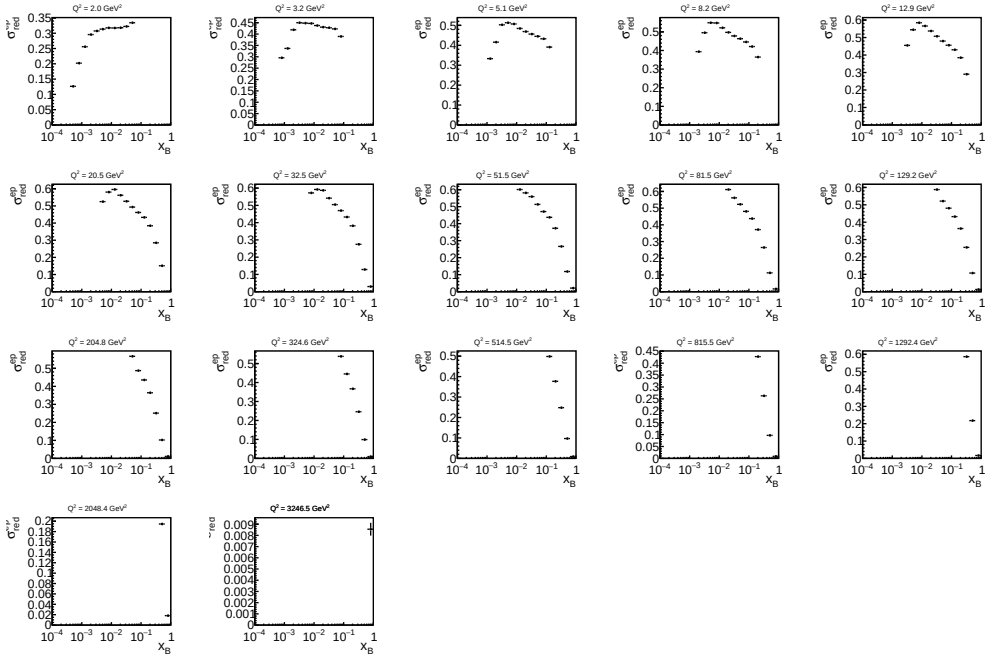

Figure 2.4: Projected *ep* neutral current reduced cross sections at 10x100 GeV. Statistical uncertainties assume an integrated luminosity of 10 fb^{-1}.

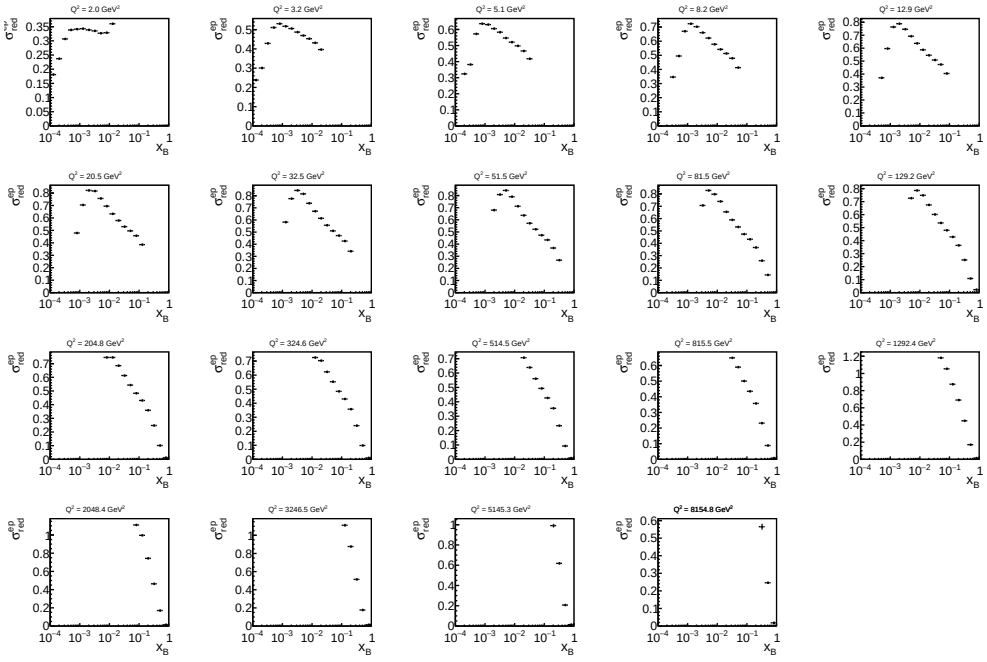

Figure 2.5: Projected ep neutral current reduced cross sections at 18x275 GeV. Statistical uncertainties assume an integrated luminosity of 10 fb^{-1}.

fb^{-1} for each center of mass energy, equally split between the the beam polarization configurations required for the asymmetry measurement. The reconstruction, event selection, and kinematic cuts are described in Sec. 2.3.2.

When extracting the double spin asymmetries for semi-inclusive measurements, $A_1^{p,h}$, the selection of final state hadrons, h, provides further sensitivity to the flavor of the struck parton. Given that DIS is generally u-quark dominated, the detection of a negative pion or a kaon with high momentum fraction relative to the initial parton momentum increases the sensitivity to down quarks, and particularly strange quarks. The role of sea quarks and particularly strange quarks in the decomposition of the proton spin is still only poorly understood and is in most global fits only constrained using hyperon decays and the assumption of $SU(3)_F$ symmetry. Using this assumption, the strange spin contribution is pushed toward negative values in the so far inaccessible region. The ePIC measurements will be able to access its contribution over a wide range in x and determine whether these symmetry assumptions are really valid. Similarly, the contributions by sea quarks can be determined using semi-inclusive DIS.

The expected precision for pions as a function of x in bins of Q^2 and momentum fraction z is shown in Fig. **??**.

2.4.3 Multi-Dimensional Imaging of the Nucleon

One-dimensional PDFs reveal the distribution of longitudinal parton momenta in the direction of the nucleon momentum. Nevertheless, a fast moving nucleon has still sizable transverse spatial dimensions.

The 3D parton structure of hadrons in momentum space is encoded in transverse momentum de-

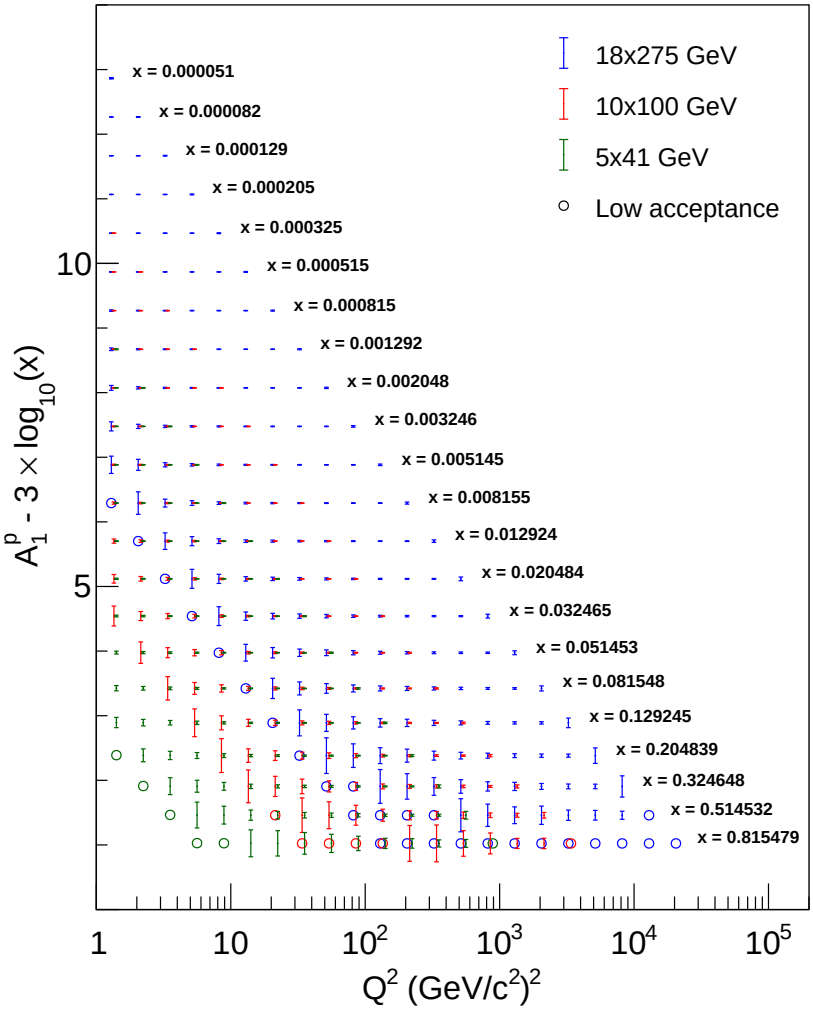

Figure 2.6: Projected measurements of A_1^p.

Figure 2.7: Projected measurements of $A_1^{p\pi^+}$ as a function of x in bins of Q^2 and momentum fraction z.

pendent parton distributions (TMDs). The non-perturbative quantities that encode the spatial distributions in the transverse plane are called generalized parton distributions (GPDs).

2.4.3.1 Imaging in Momentum Space

Using semi-inclusive DIS, it is possible to extract information on the three-dimensional momentum structure of the nucleon by making use of transverse momentum dependent parton distribution functions (TMDs-PDFs or shortly TMDs). Depending on the polarization of the nucleon and the parton within the nucleon, there are in total 8 twist-2 TMDs, while the 16 TMDs, which exist at the twist-3 level, also take quark-gluon correlations into account. Table 2.1 provides an overview on the TMDs up to twist-3.

N \q	**U**	**L**	**T**		twist 3
U	f_1		$h_1^\perp$		$f^\perp, g^\perp, h, e$
L		g_{1L}	$h_{1L}^\perp$		$f_L^\perp, g_L^\perp, h_L, e_L$
T	$f_{1T}^\perp$	g_{1T}	$h_1, h_{1T}^\perp$		$f_T, f_T^\perp, g_T, g_T^\perp, h^\perp, e_T, h_T^\perp, e_T^\perp$

Table 2.1: The 8 twist-2 and the 16 twist-3 TMDs and their dependence on the nucleon N and the quarks q polarisation (unpolarized: U, longitudinally polarized: L, transversely polarized: T).

Since the semi-inclusive DIS process also involves the hadronization of the parton which is kicked out of the nucleon during the scattering process, the observables are typically sensitive to a convolution of a TMD and a fragmentation function (FF), which describes this hadronization. These fragmentation functions are typically studied in hadron production in e^+e^- collisions, like at BELLE or BESIII, where they can be accessed in a clean way [8].

The measurement of cross sections and their angular modulations as well as beam, target and double spin asymmetries in semi-inclusive DIS, allows us to access a series of model independent structure functions, which can be directly related to a convolution of different TMDs and and FFs [9, 10]. The measurement of different hadrons in the final state allows a flavor separation of the TMDs. Besides the classical DIS variables Q^2 and x_B, semi-inclusive DIS observables are typically studied in terms of the energy fraction of the virtual photon carried by the outgoing hadron z and the transverse momentum of the outgoing hadron relative to the virtual photon direction P_T to access the full kinematic dependence of the TMDs.

For all SIDIS measurements, a few key requirements have to be fulfilled by the ePIC detector. First of all, an excellent particle identification over an as large as possible fraction of the kinematic and angular range of the scattered electrons and hadrons is required, since no exclusivity variables are available to further constrain the final state. Here especially a good pion to Kaon and proton separation up to high momenta is desirable. Furthermore, a differential binning of the observables in terms of the relevant kinematic variables requires a good momentum resolution to reduce distortions from bin migration effects. Both aspects will directly affect the achievable systematic uncertainties and therefore the total precision of the measurement.

Already with an un-polarized nucleon the ePIC experiment can provide flavor-separated TMDs over a large range in x_B and Q^2, and for transverse momenta that reach from the low, TMD-dominated region into the perturbative region. The wide range of scales, as shown in Fig.2.8 (left) will also solve the existing uncertainties in the TMD evolution where non-perturbative contributions require experimental input. As shown in Fig.2.8 (right), the data expected from ePIC will significantly reduce the uncertainties of the extraction of unpolarized TMDs over most of the kinematic range.

The unpolarized TMD PDFs also serve as the unpolarized baseline for any polarized TMD observable which are obtained as single or double spin asymmetries. The most relevant are the Sivers function $f_{1T}^\perp$ [11,12] and the quark transversity $h_1^\perp$ which is obtained together with either the Collins fragmentation function or a di-hadron fragmentation function. Examples of the expected uncertainties on these asymmetries are displayed in Fig. 2.9 where one can see that over a larger range of phase space very precise uncertainties can be obtained. Those will in turn then provide flavor-separated Transversity extractions and their first moments, the tensor charges. These tensor charges are of particular interest as they can relate to interactions outside the standard model. Lattice-QCD can model the tensor charges very well and any differences with the measurements would provide a hint for BSM physics.

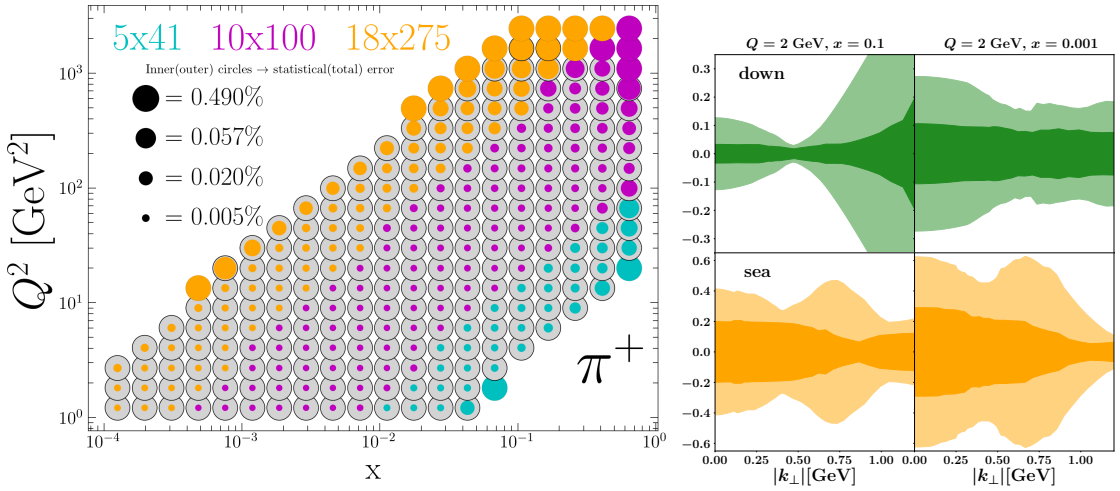

Figure 2.8: Left: Expected statistical and total uncertainty of un-polarized TMD PDFs for π^+ in the $Q^2 - x_B$ plane. The inner (colored) circle shows the statistical uncertainty, while the outer circle provides the total uncertainty for each $Q^2 - x_B$ bin. The color shows the beam energy configuration which provides the highest statistics in a specific bin. Right panel: Expected uncertainties of valence down (green) and sea quark (orange) TMD PDFs at $x = 0.1$ (left) and $x = 0.001$ (right) as obtained based on the MAP24 [1] global TMD fit. The lighter shaded regions show the uncertainties based on existing data while the darker shaded regions show the expected uncertainties after including ePIC data.

Collins asymmetries of identified hadrons in jets are also sensitive to the Collins Fragmentation Function (FF), which describes the azimuthal distribution of hadrons fragmented by a transversely polarized quark as a function of the parent quark momentum fraction carried by the hadron (z) and the hadron momentum transverse to the quark direction (κ_T). Figure 2.10 illustrates projected statistical precision for Collins asymmetry measurements of charged π, K and p in jets as a function of hadron z and jet p_T. An absolute statistical uncertainty of less than XXX can be achieved for jet $p_T = 20$ GeV/c for protons. When integrated over jet $5.0 < p_T < 51.9$ GeV/c, the statistical uncertainty becomes negligible for the range of $0.1 < z < 0.8$. These high precision measurements will provide stringent constraints for quark transversity in the proton.

2.4.3.2 Imaging in Transverse Position Space

As introduced earlier, GPDs can be extracted via measurements of exclusive reactions. e.g. the exclusive production of a real photon via DVCS or of a meson, while the proton remains intact. Exclusivity requires all the final-state particles to be detected.

DVCS events have been simulated using the EpIC Monte Carlo generator [13] with a minimum Q^2 of 1 GeV^2. The analysis of such events provides a good test of a large number of subsystems within the ePIC detector, namely the scattered electron and final state photon are detected in either the central barrel or endcaps, and the scattered proton is detected in the far forward region within the B0 spectrometer or the Roman Pot detectors.

DVCS candidate events were identified by applying a series of cuts on the individual final state particles, as well as on the properties of the full reaction. The cuts applied were as follows:

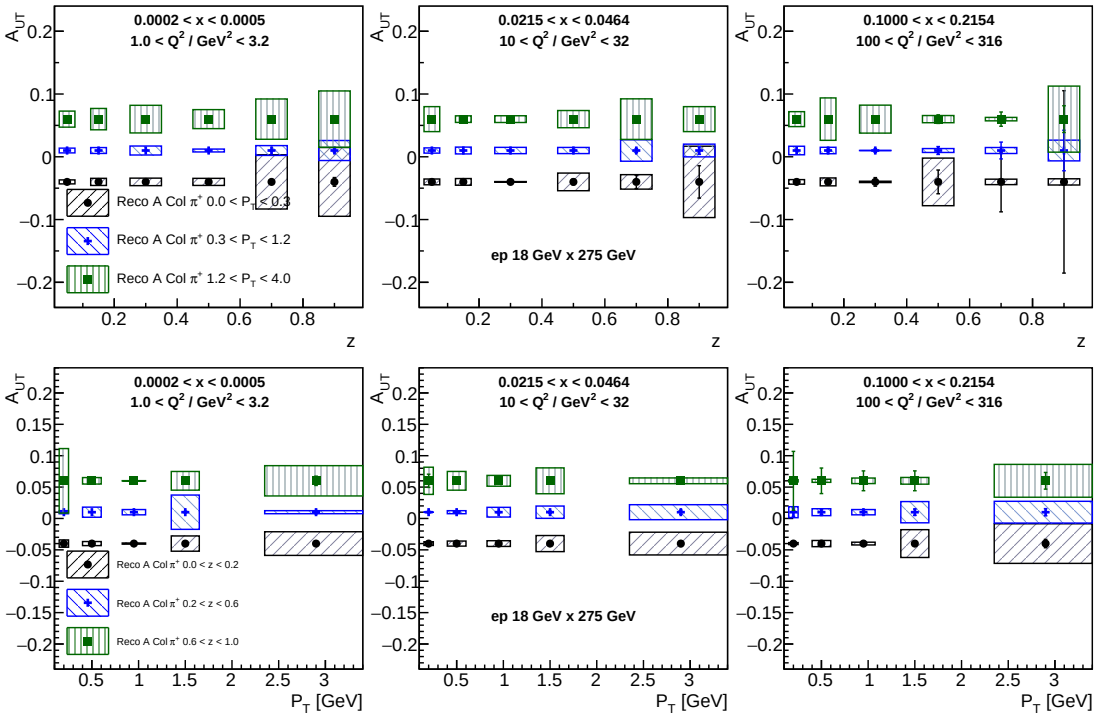

Figure 2.9: Top: Expected uncertainties in three example x-Q^2 bins for the Collins asymmetries for positive pions as a function of the momentum fraction z and in three bins of hadron transverse momentum relative to the virtual photon direction assuming a luminosity of 10 fb^{-1}. Bottom, the same but as a function of the hadron transverse momentum in bins of z.

- exactly 1 photon, scattered electron and scattered proton were reconstructed in the final state.
- the reconstructed electron and photon have momenta no more than 10% higher than the corresponding beam momentum; for this study, that corresponds to a maximum of 11 GeV for scatterd electrons and 110 GeV for scattered protons.
- track θ cuts for the reconstructed proton (where θ is defined as the angle from the positive z-axis to the track of interest) to ensure the track matches the acceptance of the detector expected. Tracks reconstructed in the Roman Pots are required to have $\theta < 5.5$ mrad; tracks in the B0 spectrometer are required to have $5.5 < \theta < 20$ mrad.
- a minimum Q^2 of 1 GeV^2, to match the conditions of the initially generated events.
- a maximum t for events with the proton detected in the Roman Pots of 0.3 GeV^2.
- a maximum missing mass of the full final state, M^2_{miss} of 1 GeV^2.

As mentioned, a key parameter on which the DVCS process depends is the Mandelstam variable t of the reaction. The generated and reconstructed distributions of t, calculated for events with full exclusivity (exactly one reconstructed electron, proton and photon), are shown in figure 2.11. As well as studying the underlying physics process, DVCS can be used to test the performance of the ePIC subdetectors. Figure 2.12 shows the angular resolution of the barrel calorimeters, calculated using the detected DVCS photon. Of particular note from figure 2.12 are the following points:

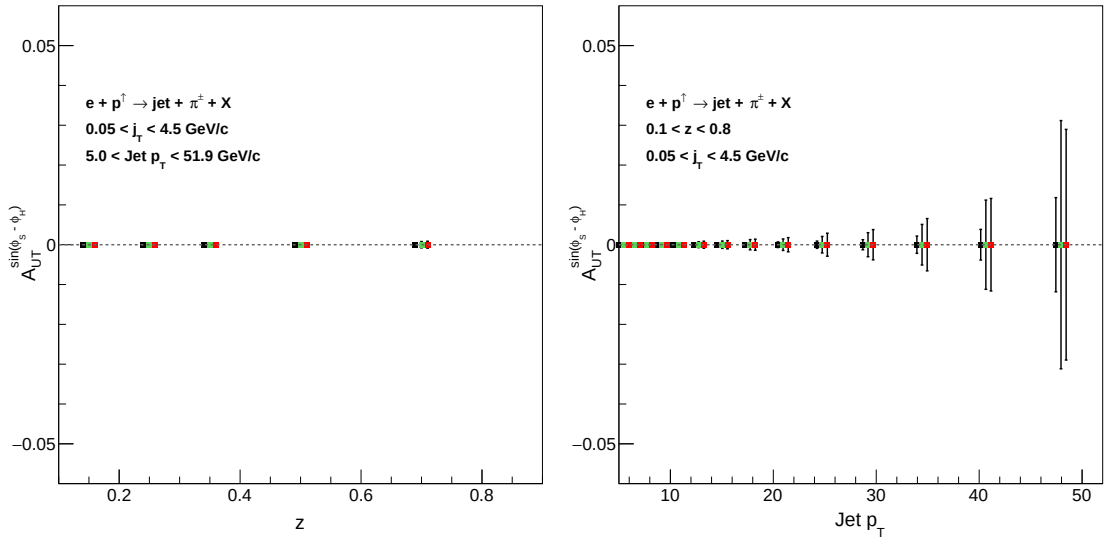

Figure 2.10: Projected statistical precision, indicated by vertical bars around data points, for measurements of Collins asymmetries of identified hadrons in jets as a function of hadron z (left) and jet p_T (right). In case the vertical bars are invisible, they are smaller than the marker size. This figure will be updated

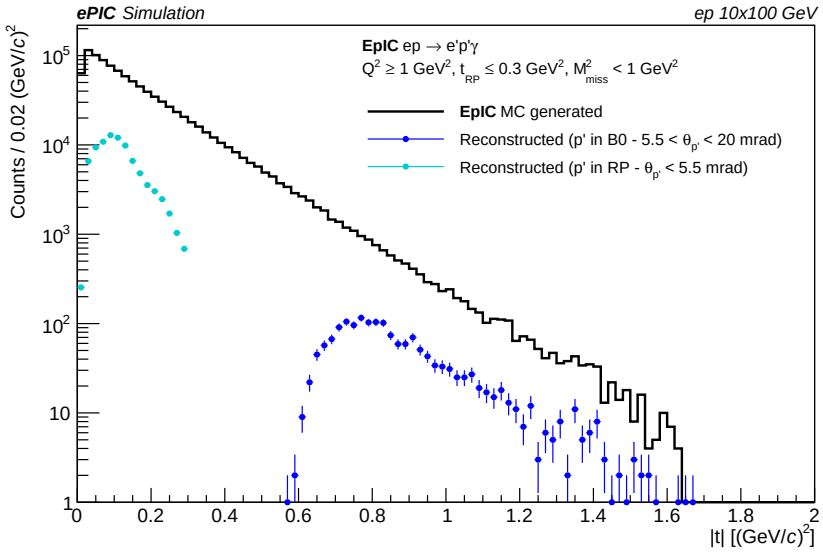

Figure 2.11: Generated and reconstructed t-distributions for fully-exclusive DVCS events.

- the angular reconstruction of the barrel is, on the whole, very good. No more than 0.5% of all photons are reconstructed more than 5° from their generated track, and more than 75% are reconstructed to within 1°.
- the significant majority of the generated photons are detected in the electron endcap calorimeter, in the range $2.8 < \theta < 3.1$ rad.

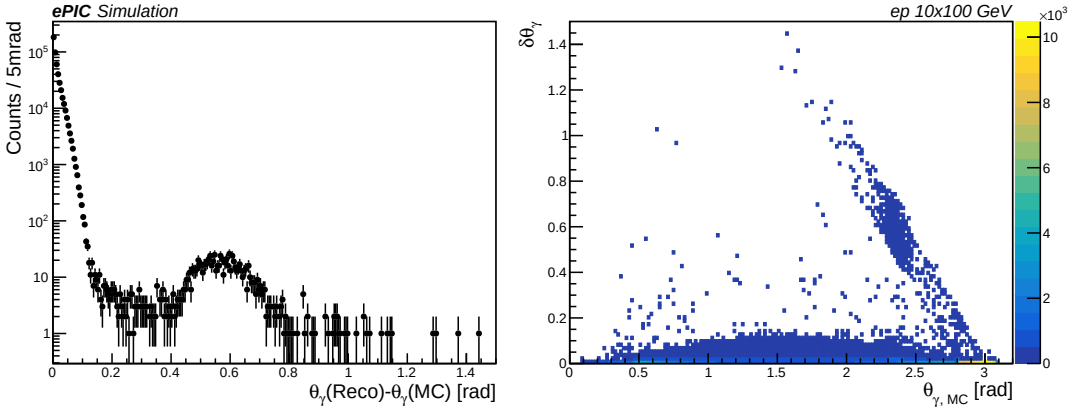

Figure 2.12: Reconstructed minus generated track θ for all reconstructed DVCS photons (left), as well as as a function of the generated photon θ (right). Note that the left plot is on a logarithmic scale.

Overall, based on the feasibility study, this measurement can be fully carried out by the ePIC detector. In particular, the study on DVCS is sensitive to the performances of both the far-forward detector system, especially the B0 and Roman Pot, as well as the Barrel Imagining Calorimeter, which are both discussed in more details in Chapter 8.

2.4.3.3 Upsilon production

The study of exclusive heavy quarkonia production is an excellent tool for investigating quantum chromodynamics (QCD) at the Electron-Ion Collider (EIC). Due to the heavy masses of both charm and bottom quarks, which are significantly greater than Λ_{QCD}, studying heavy quarkonia enables QCD research in the perturbative regime, facilitating the exploration of gluon PDFs [14]. Numerous studies have employed ultraperipheral collisions (UPCs) to examine the properties of heavy quarkonia and their implications for QCD [15–18].

In lowest order perturbative QCD, the cross-section for exclusive heavy meson production is proportional to the square of the gluon density, at a $Q^2 = (M_V/2)^2 + Q^2_\gamma$, while the Bjorken$-x$ depends on the photon energy; at low Q^2, $x = M_V/\gamma m_p exp(y)$, where γ is the Lorentz boost of the ion, and y is the final state rapidity. So, it serves as an important probe of gluons at low$-x$, with the lowest x gluons being probed at large y. Wide y coverage is important to probe the lowest x values. The interest goes beyond just the cross-section; $d\sigma/dt$ for coherent production is sensitive to the transverse distribution of gluons in the target, while incoherent production may be sensitive to nuclear fluctuations, including gluonic hotspots [19].

Among vector mesons, the Υ is particularly attractive. At next-to-leading order, quarks also contribute to vector meson production, but the quark contribution to Υ production is much smaller than for the J/ψ [20]. And, the theoretical uncertainties due to scale and other factors are much smaller for the Υ than for the J/ψ [20, 21].

The Υ states are notable as the heaviest vector mesons accessible at the EIC, allowing to probe a high intrinsic Q^2. The three different Υ states are all composed mainly of $b\bar{b}$, but have three different wave functions; thus, by comparing production of the three states, it will be possible to

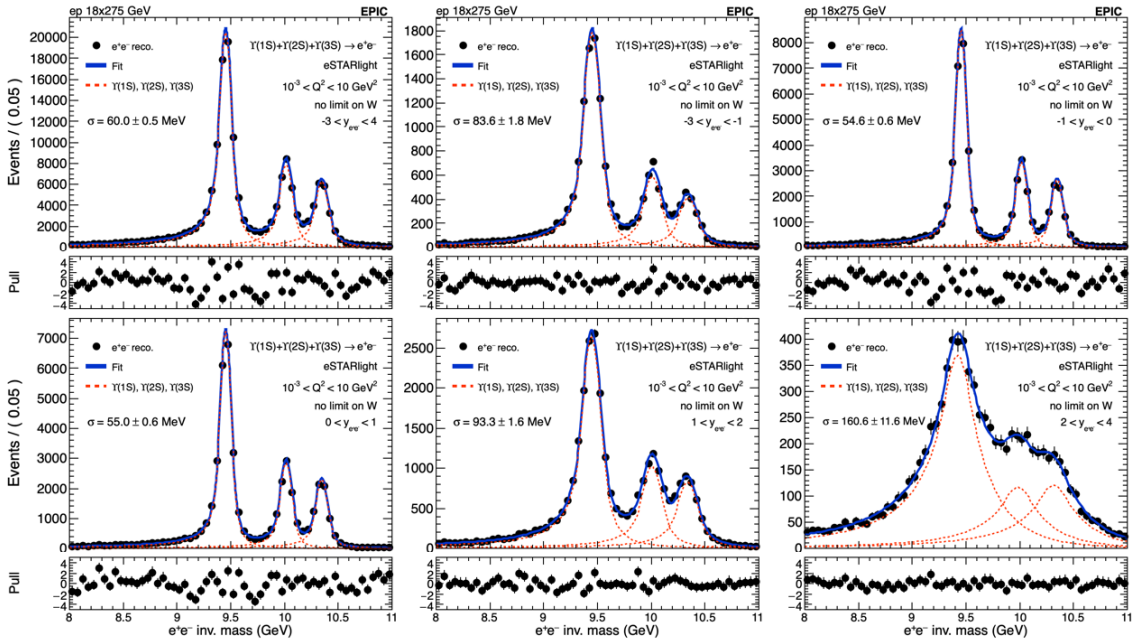

Figure 2.13: The reconstructed mass distribution of the Υ three states in the electron channel from the electron-proton collisions at $18 \times 275\ GeV$, utilizing the tracker with realistic seeding. The top left plot shows the invariant mass distribution of the Υ three states in the rapidity range from -3 to 4. The other plots display invariant mass distribution for specific rapidity intervals: (top middle) $-3 < y < -1$, (top right) $-1 < y < 0$, (bottom left) $0 < y < 1$, (bottom middle) $1 < y < 2$, and (bottom right) $2 < y < 4$. The resolution of the Υ three states is indicated on each plot as σ.

reduce the systematic uncertainties on the gluon distribution extraction.

The production of the three Υ states in the electron channel was simulated in electron-proton collisions at a center-of-mass energy of 18×275 GeV. The Monte Carlo samples were generated using eSTARlight, covering a range of $10^{-3} < Q^2 < 10\ GeV^2$, with no restrictions on W. The Υ states were produced according to their relative ratio based on [22] and then combined. The reconstruction of these Monte Carlo samples was simulated using EICRECON version 1.15.0. The figure showcases the momentum resolution of the ePIC tracking system in terms of separating the three Υ states, which is presented across various rapidity regions for the reconstructed Υ states. The top left plot in Figure 2.13 represents the resolution for all rapidity regions combined, while the other plots present results for specific intervals: $-3 < y < -1$, $-1 < y < 0$, $0 < y < 1$, $1 < y < 2$, and $2 < y < 4$. In the forward region, corresponding to $2 < y < 4$, a degradation in resolution was observed. However, in a similar study done by the muon channel (not shown), it is found to have an improvement on the resolution of approximately 1 to 8 % due to reduced final state radiation. Additionally, these studies help assess detector performance, particularly the momentum resolution of the tracking system.

2.4.4 Properties of Nuclear Matter

2.4.4.1 Gluon Saturation

One of the three central questions highlighted in the National Academy of Science report on Electron-Ion Collider (EIC) science is to understand the properties of high parton density matter and the onset of gluon saturation. A critical observable for understanding the dynamics of gluonic matter is the spatial distribution of gluons within nuclei, particularly in systems likely to be in the saturation regime at high energy.

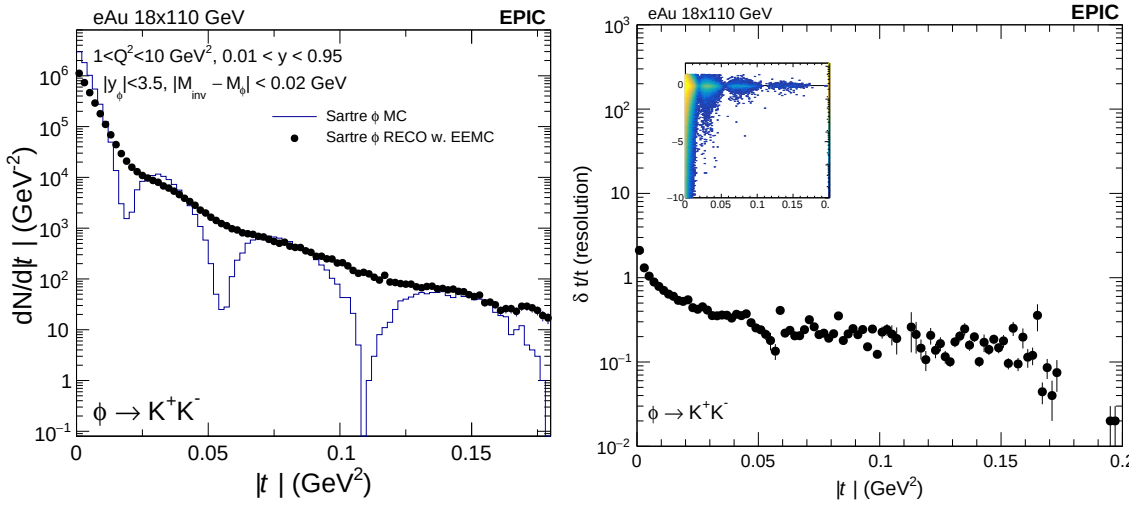

Figure 2.14: Left: differential distribution of the momentum transfer $|t|$ of coherent ϕ meson electroproduction in electron-gold collisions with 18x110 GeV. The Monte Carlo model is provided by Sartre and the reconstructed distribution is obtained from full ePIC simulation with the official August 2024 simulation campaign. Right: the momentum transfer t reconstruction resolution as a function of the true t.

To achieve gluon imaging of nuclei, exclusive and diffractive vector meson electroproduction involving electron-heavy nuclei collisions has been proposed [4]. In Fig. 2.14 (left), the differential cross section for ϕ meson production is shown for electron-gold collisions at an energy configuration of 18x110 GeV. The input is derived from the Monte Carlo model Sartre, and the reconstructed distribution is obtained after a full ePIC simulation based on the version from August 2024. The reconstruction is achieved by detecting a scattered electron in the backward calorimeter and reconstructing the two kaons from ϕ decay using tracking data.

As shown, the diffractive structure is barely visible in the reconstructed data due to insufficient momentum transfer (t) resolution. The main limitation stems from the electron reconstruction, where the momentum resolution is hampered by the small scattering angle relative to the electron beamline. The magnetic field in this region is insufficient to provide the necessary lever arm for achieving the required momentum resolution. More specifically, Fig. 2.14 (right) presents the momentum transfer t reconstruction resolution as a function of true t. Efforts to improve the resolution are ongoing.

On the other hand, the incoherent vector meson production needs to be vetoed in the event in order

	Signal efficiency	Background efficiency
3 tracks	0.97383	0.914885
J/ψ mass window	0.898815	0.827045
Veto signals in B0	0.898805	0.429656
Veto signals in OMD	0.898805	0.29286
Veto signals in ZDC	0.898795	0.013776

Table 2.2: Event composition in incoherent J/ψ production before and after full event selection

to suppress its contamination to the coherent process. This is enabled by the far-forward detector system (B0, Roman Pot, Off-Momentum Detector, zero-degree calorimeter). By vetoing signals in the forward detectors one can reject up to two orders of magnitude of the incoherent background. Table 2.2 summarizes the fraction of signal and background events after each veto.

The t spectra of coherent and incoherent (before veto) are shown in Fig. 2.15 left, and the residue distribution of incoherent production events (that pass event selection) are shown in Fig. 2.15 right. Therefore, the vetoing power is sufficient to supress the incoherent production down to a level below the first diffractive minimum but not quite for the second and third minima.

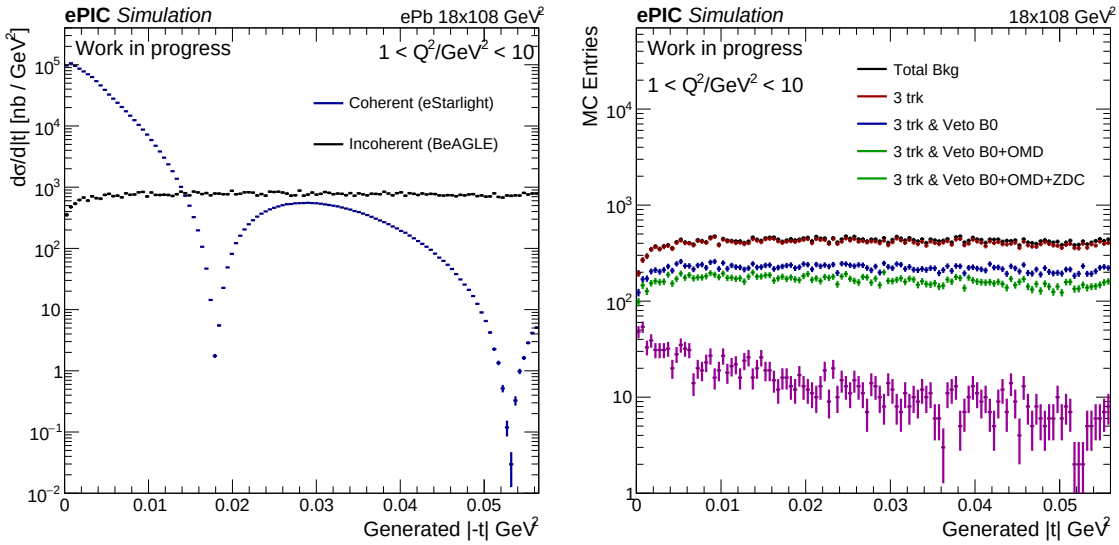

Figure 2.15: Left: Differential cross-section of momentum transfer t distribution for coherent (blue) and incoherent (black) exclusive J/ψ production in ePb collisions. Right: Differential measurement of t and the residue distributions after each veto based on the far-forward detector system.

2.4.4.2 Nuclear Modifications of Parton Distribution Functions

Add text here.

2.4.4.3 Passage of Color Charge Through Cold QCD Matter

[Rongrong: performance of D^0 reconstruction with ePIC is currently under study. It will not be available for pre-TDR. We are aiming to include it in TDR.]